Jpn. J. Appl. Phys. Vol. 38 (1999) pp. 4056–4064
Part 1, No. 7A, July 1999

Aggregation Effect on the Third-Order Optical Nonlinearity in 4-(N,N-Diethylamino)-β-Nitrostyrene-Doped Polymer Films

Hidetoshi MURAKAMI[1,*], Ryuji MORITA[1,3], Mikio YAMASHITA[1,3] and Hidemi SHIGEKAWA[2,3]

[1]*Department of Applied Physics, Hokkaido University, Kita-13, Nishi-8, Kita-ku, Sapporo 060-8628, Japan*
[2]*Institute of Materials Science, Center for Tsukuba Advanced Research Alliance, University of Tsukuba, 1-1-1 Tennodai, Tsukuba 305-8573, Japan*
[3]*CREST, Japan Science and Technology Corporation (JST)*

(Received November 16, 1998; revised manuscript received April 1, 1999; accepted for publication April 22, 1999)

The absorption and electroabsorption (EA) spectra for 4-(N,N-diethylamino)-β-nitrostyrene (DEANST)-doped poly(methyl methacrylate) (PMMA) films in the dopant concentration range of 0.1–40 wt% were measured. Dispersion of the third-order nonlinear optical susceptibility $\chi^{(3)}(-\omega; 0, 0, \omega)$ at each concentration was determined. In addition, the static polarizability change $\Delta\alpha$ and the static dipole-moment change $\Delta\mu$ were evaluated. Furthermore, the picosecond emission-decay profiles and the time-resolved emission spectra for 0.1–40 wt% DEANST-doped PMMA films were measured. From the experimental results, it was concluded that DEANST molecules in PMMA films aggregate at concentrations over 5 wt%. This aggregation gives rise to two new absorption bands. The intermolecular interaction affected by aggregation causes a decrease in $\Delta\mu$, in the average effective third-order molecular hyperpolarizability $\langle\gamma(-\omega; 0, 0, \omega)\rangle_{\mathrm{eff}}$, and in the nonproportional behavior in $|\chi^{(3)}(-\omega; 0, 0, \omega)|$ with increasing dopant concentration. Furthermore, this aggregation explains the absorption spectral change, the EA spectral shift and the existence of two emission-decay constants with concentration. Finally, the average aggregation number of DEANST molecules was evaluated to be two, which suggests that DEANST molecules in the PMMA film form a dimer at concentrations over 5 wt%.

KEYWORDS: charge-transfer molecule, nonlinear organic material, polymer, electroabsorption, third-order optical nonlinearity, time-resolved emission spectrum, aggregation, dimer

1. Introduction

Organic materials with π-conjugated electron systems have received considerable attention because of their high optical nonlinearities. It is known that, among those materials, the organic molecules possessing the structure of donors and acceptors substituted into the π-conjugated system have higher optical nonlinearities, owing to the intramolecular charge transfer. The present work concerns one of those materials, 4-(N,N-diethylamino)-β-nitrostyrene (DEANST).[1)] In a DEANST molecule, a diethylamino group as a donor, and a nitroehtylene group, as an acceptor, are attached to each side of the aromatic ring, thus a DEANST molecule has a large third-order hyperpolarizability, high solubility and good crystallinity. Therefore, the extremely high solubility of DEANST in polar solvents and in poly(methyl methacrylate) (PMMA) films[2)] makes us expect a material with a large third-order nonlinear optical susceptibility $\chi^{(3)}$ proportional to the concentration. However, this linear relationship between $\chi^{(3)}$ and concentration is not always self-evident at high concentrations. In particular, at extremely high concentrations, the mechanism of the third-order optical nonlinearity can be different from that at typical concentrations, even for a concentrated system which does not show a clear or significant change of the absorption spectrum. In general, it is difficult to clarify the difference between the third-order nonlinear mechanism of monomers and that of a lower degree of aggregates, such as dimers, in the same solvent, where absorption spectra almost overlap each other, unlike in the case of J-aggregates.[3)] This may be one of the reasons why the nonlinear optical investigation of the molecular system, in which absorption-spectrum-overlapping monomers and dimers coexist, has rarely been carried out so far.

Modulation absorption spectroscopy using an external electric field is a powerful technique for the investigation of the subtle differences between the electronic structures of a complex compound. The permanent dipole moment and linear polarizability are key parameters that govern nonlinear optical constants as well as linear optical constants. From the measurement of electroabsorption, we can evaluate the change in those parameters for the electronic transition from a ground to an excited state.[4)] Moreover, we can determine the dispersion of the third-order nonlinear optical susceptibilities $\chi^{(3)}(-\omega; 0, 0, \omega)$ through the Kramers-Kronig relation.[5,6)] Thus we can clarify the origin of the nonlinearities.

The purpose of the present work is to clarify the mechanism of the third-order optical nonlinearity in DEANST-doped PMMA films at low and high dopant concentrations. The optical nonlinearity is investigated as a function of the dopant concentration over a wide range from 0.1 to 40 wt%, using modulation absorption spectroscopy. The picosecond time-resolved emission spectroscopy is also applied to reveal the difference between the excited-state relaxation processes at low concentrations and at high concentrations. As a result, it is shown that at high concentrations over 5 wt%, aggregates which reduce the effective third-order hyperpolarizability are formed, and hence third-order susceptibility is not proportional to the concentration of DEANST molecules.

2. Experimental and Analysis

2.1 Sample preparation

DEANST was synthesized based on ref. 1 and purified by recrystallization by a slow-cooling method. PMMA (Aldrich) was used as a host material. Conductive indium-tin-oxide (ITO)-coated quartz glass was employed as a substrate. The polymer solution with DEANST was spin-coated on the substrate and then dried at room temperature for 5–6 h. The concentration of DEANST relative to the weight of PMMA was varied in the range of 0.1–40 wt%. Semitransparent aluminum was deposited on the film surface as a counterelectrode. A typical sample thickness was about 0.1–0.2 μm, which was measured by multiple-beam interferometry (Mi-

*mhide@eng.hokudai.ac.jp

zojiri BM-4).

2.2 *Experimental setup*

We performed two types of measurement: electroabsorption spectroscopy measurement and picosecond time-resolved emission measurement. All the measurements were carried out at room temperature. As shown in Fig. 1, the measuring system for electroabsorption spectroscopy consists of a 150 W Xe-arc lamp (Hamamatsu Photonics), a grating monochromator (Oriel 77250, the wavelength resolution is 1 nm), appropriate color filters to cut off the second-order diffraction light, and a photomultiplier tube (Hamamatsu Photonics, H5783-06) to detect a signal. In the electroabsorption measurement, a sinusoidal ac electric field with a modulation frequency of ~1 kHz and a field strength on the order of 10^5 V/cm was applied to the sample. The field-induced change in absorption intensity was detected by a lock-in amplifier (Stanford Research Systems, SR-830) at the second harmonic of the modulation frequency. The measurement was performed in the range of 2.07 eV (600 nm) to 3.59 eV (345 nm).

The experimental setup for the time-resolved emission measurement was similar to the previously employed one.[7] The light source was a mode-locked Ti:sapphire laser (Clark) pumped by an Ar-ion laser (Coherent, Innova 310). The pulse duration was about 100 fs centered at around 790 nm. The average power at a 100 MHz repetition rate was about 1 W. The second-harmonic wave (395 nm, ~ 200 fs), generated by frequency conversion from the fundamental wave using a lithium triborate (LBO) crystal, was used as an excitation light of the sample. The typical average power of the excitation pulses was 50 mW. The signal was detected by a synchroscan streak camera (Hamamatsu Photonics, M1955) attached to a polychromator. The measured wavelength range for all samples was 1.98–2.62 eV (627–473 nm) and the time resolution was ~3 ps.

2.3 *Determination of* $\chi^{(3)}(-\omega; 0, 0, \omega)$ *and* $\gamma(-\omega; 0, 0, \omega)$ *dispersions*

The third-order nonlinear optical susceptibility $\chi^{(3)}(-\omega; 0, 0, \omega)$ can be calculated from absorption spectra $A(\omega)$, Kerr-effect electroabsorption spectra $\Delta A(\omega)$, refractive index $n(\omega)$ and refractive index change $\Delta n(\omega)$.[5,6] The refractive index $n(\omega)$ is related to the absorption coefficient through the Kramers-Kronig (K-K) relation, and the refractive index change $\Delta n(\omega)$ due to electromodulation can be obtained using the following derivative form of the K-K relation,

$$\Delta n(\omega) = \frac{c}{\pi}\mathcal{P}\int_0^\infty \frac{\Delta A(\omega')}{\omega'^2 - \omega^2} d\omega', \tag{2.1}$$

where $\mathcal{P}$ denotes the Cauchy principal value of the integral and c is the velocity of light. This relation is valid for the case where the frequency of the applied electric field is low and the system can be regarded to be in a steady state. The third-order nonlinear optical susceptibility $\chi^{(3)}(-\omega; 0, 0, \omega)$ can be expressed by

$$\chi^{(3)}(-\omega; 0, 0, \omega) = \frac{1}{6\pi F^2}[(n(\omega)\Delta n(\omega) - k(\omega)\Delta k(\omega)) + i(n(\omega)\Delta k(\omega) + k(\omega)\Delta n(\omega))], \tag{2.2}$$

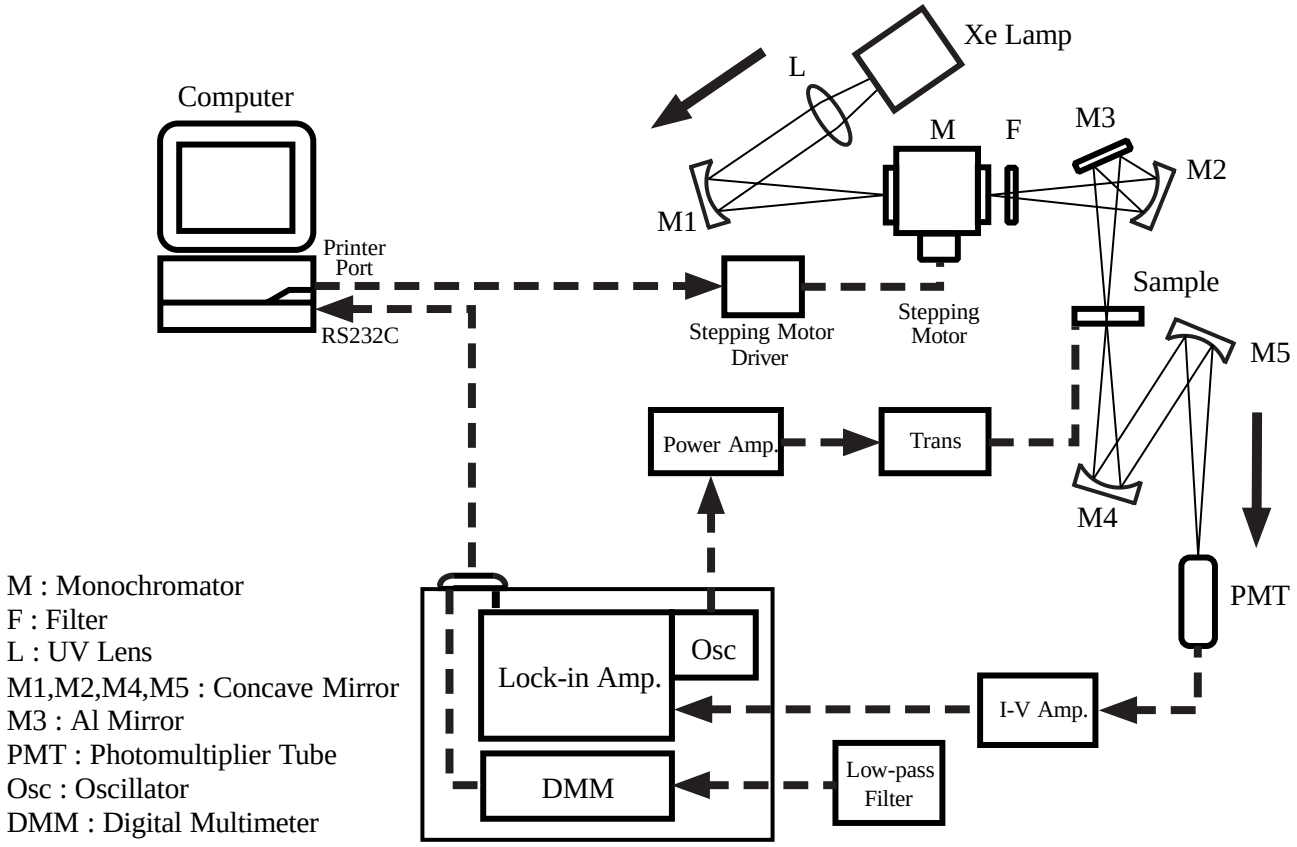

Fig. 1. Experimental setup for electroabsorption measurement.

where F is the amplitude of the applied electric field and k and Δk are the extinction coefficient and its change due to electromodulation, respectively, represented by

$$k(\omega) = \frac{\lambda}{4\pi} A(\omega), \tag{2.3}$$

$$\Delta k(\omega) = \frac{\lambda}{4\pi} \Delta A(\omega), \tag{2.4}$$

where λ is the wavelength.

The average third-order hyperpolarizability $\langle \gamma(-\omega; 0, 0, \omega) \rangle$ is expressed by

$$\langle \gamma(-\omega; 0, 0, \omega) \rangle = \frac{\chi^{(3)}(-\omega; 0, 0, \omega)}{N L(0)^2 L(\omega)^2}, \tag{2.5}$$

where N is the molecular number density. Here $L(\omega)$ is the Lorentz local-field factor given by

$$L(\omega) = \frac{\epsilon(\omega) + 2}{3}, \tag{2.6}$$

where ϵ is the dielectric constant.

2.4 Derivation of static dipole-moment change and static polarizability change

When an electric field is applied to isotropic samples, the change in absorption spectrum can be described by a linear combination of an absorption spectrum and its first and second derivatives, as follows:[4,8,9]

$$\Delta A(E, F)/E = \left[a_0 \left(\frac{A}{E} \right) + a_1 \frac{d}{dE} \left(\frac{A}{E} \right) + a_2 \frac{d^2}{dE^2} \left(\frac{A}{E} \right) + \cdots \right] R(\theta) [L(0)F]^2, \tag{2.7}$$

where E is the photon energy. a_0, a_1 and a_2 are, respectively, given by

$$a_0 = \frac{X^2}{\mu_{ng}^2} + \frac{2Y}{\mu_{ng}}, \tag{2.8}$$

$$a_1 = \frac{2X}{\mu_{ng}} \Delta\mu + \frac{1}{2} \Delta\alpha, \tag{2.9}$$

$$a_2 = \frac{1}{2} (\Delta\mu)^2, \tag{2.10}$$

where $\Delta\mu$ and $\Delta\alpha$ are the permanent-dipole-moment difference and the linear-polarizability difference between an excited state and a ground state. Here, μ_{ng}, X and Y are the transition-dipole moment, the transition-dipole-moment polarizability and its hyperpolarizability, respectively. They have a relationship expressed in the dyadic notation

$$\boldsymbol{\mu}_{ng}(\boldsymbol{F}_{\text{int}}) = \boldsymbol{\mu}_{ng} + \mathsf{X} \cdot \boldsymbol{F}_{\text{int}} + \boldsymbol{F}_{\text{int}} \cdot \mathsf{Y} \cdot \boldsymbol{F}_{\text{int}} + \cdots, \tag{2.11}$$

where $\boldsymbol{F}_{\text{int}}$ is the internal electric field ($\boldsymbol{F}_{\text{int}} = L(0)\boldsymbol{F}$). In eqs. (2.8)–(2.10), we assume that all the electric properties of DEANST are dominated by only one component along the Z-axis (Z-axis is defined as the long axis of the DEANST molecules). Namely, the vectors $\boldsymbol{\mu}_{ng}$ and $\Delta\boldsymbol{\mu}$, the tensors X and Y and $\Delta\boldsymbol{\alpha}$ can be expressed by $\mu_{ng,z}$, $\Delta\mu_z$, X_{zz}, Y_{zzz} and $\Delta\alpha_{zz}$, respectively. Thus, we use the scalar notation μ_{ng}, $\Delta\mu$, X, Y and $\Delta\alpha$. $R(\theta)$ is a general sensitivity function given by

$$R(\theta) = \frac{1}{15} [5 + (3\cos^2\xi - 1)(3\cos^2\theta - 1)], \tag{2.12}$$

where ξ is the angle between the directions of $\boldsymbol{\mu}_{ng}$ and $\Delta\boldsymbol{\mu}$, and θ is the angle between the directions of the applied electric field and the polarization vector of the incident light. In the present study, $R(\theta)$ is reduced to 1/5 because $\xi = 0°$ and $\theta = 90°$ from the above-mentioned assumption and the configuration of the experimental setup.

The first, second and third terms in eq. (2.7) correspond to the change in oscillator strength, spectral shift and broadening induced by the applied electric field, respectively. When the change in linear polarizability is significant, the first derivative of the absorption spectrum is dominant in the electroabsorption spectrum. In contrast, when the change in the permanent dipole moment is significant, the second derivative is dominant. This formula is valid for an isolated absorption band due to a single electronic transition.

3. Experimental Results

3.1 Absorption and electroabsorption spectra

The absorption spectra for DEANST/PMMA films depend on the concentration of DEANST molecules. Figure 2 shows the absorption spectra (A) from 0.1 to 40 wt% dopant concentrations, which are scaled so that the peaks are of the same height. The first dipole-allowed electronic transition band of the DEANST molecule is at $\sim$ 2.8 eV, corresponding to the π-π^* transition.[10,11] It is noted that small shoulders, which are slightly larger on the low-energy side, appear on both sides of the absorption spectrum at dopant concentrations over 15 wt%.

Figure 3 shows the electric-field-modulated absorption (EA) spectrum for DEANST-doped PMMA thin film (DEANST/PMMA film) together with the absorption spectrum for the dopant concentration of 0.1 to 40 wt% in the region of 2.07 to 3.59 eV (600 to 345 nm). The position of the first peak of the EA spectrum is the absorption edge of the sample. The magnitude of the signal change (ΔA) induced by the electric field ($\sim 10^5$ V/cm) is on the order of 10^{-5}–10^{-4}. When the dopant concentration of the sample varies from 0.1 to 40 wt%, the EA signal shifts to the low-energy side follow-

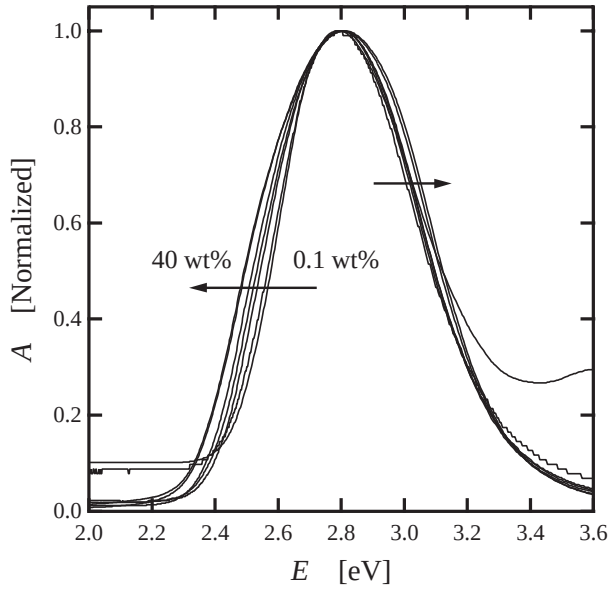

Fig. 2. Normalized absorption spectra of DEANST/PMMA films in the dopant concentration range of 0.1–40 wt%.

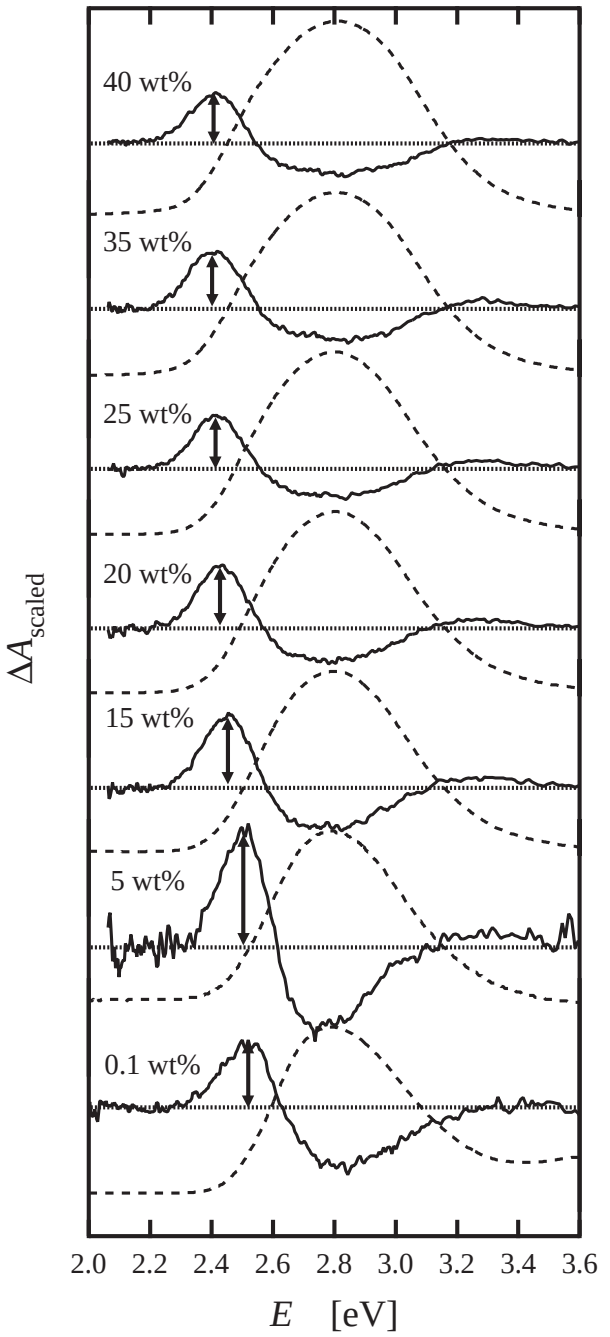

Fig. 3. The scaled EA spectra of DEANST/PMMA films (solid lines) in the dopant concentration range of 0.1–40 wt%, and corresponding absorption spectra (broken lines). All EA spectra were corrected for differences in applied field and optical density (see text).

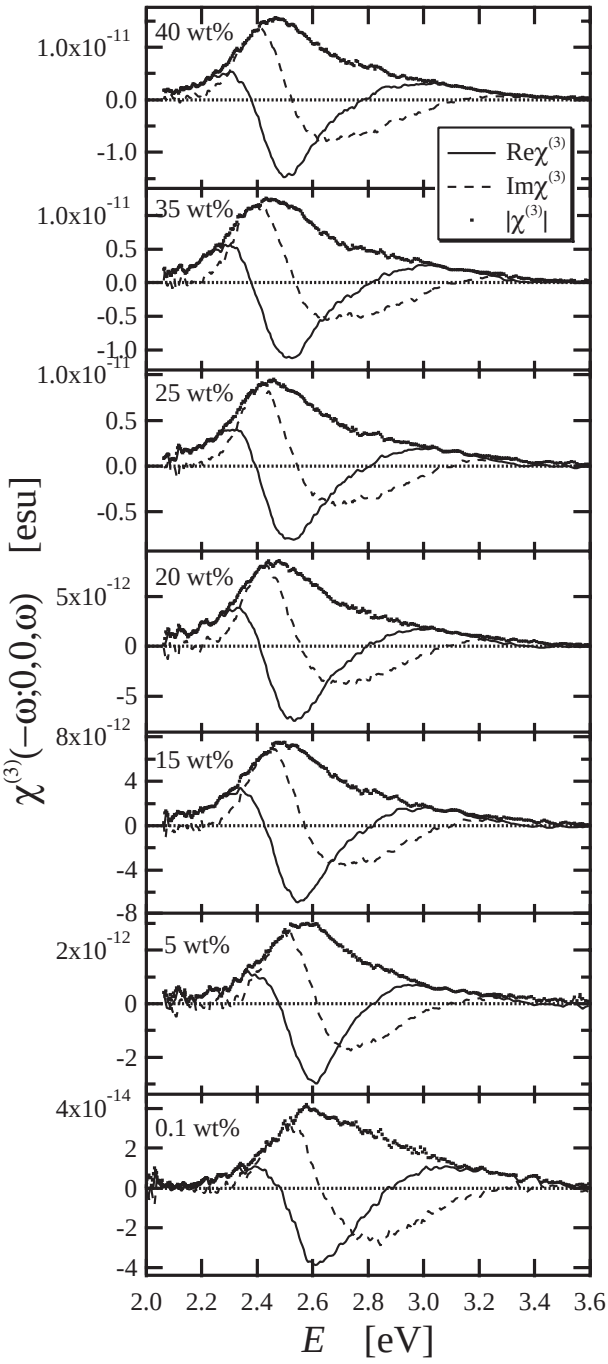

Fig. 4. Dispersion of the third-order nonlinear optical susceptibility $\chi^{(3)}(-\omega; 0, 0, \omega)$ for DEANST/PMMA films in the dopant concentration range of 0.1–40 wt%. Solid, broken and dotted lines represent the real part, imaginary part and absolute value of $\chi^{(3)}(-\omega; 0, 0, \omega)$, respectively.

ing the absorption-spectrum change. In order to compare the magnitudes of the EA signals, the spectra are normalized by the following equation:[12)]

$$\Delta A_{\text{scaled}} = \frac{\Delta A}{A_{\max} F_{\text{int}}^2}, \tag{3.1}$$

where $A_{\max}$ is the maximum value of the absorption spectrum and F_{int} is the internal electric field. ΔA_{scaled} is proportional to the interaction strength between the sample and the electric field. As the concentration of DEANST molecules increases, the magnitude of the first peak of the scaled EA signal decreases up to 15 wt%, above which, change is negligible. The changes in absorption and EA spectra with concentration reveal that the properties of DEANST in PMMA change dramatically at around the concentration of ~15 wt%.

3.2 Third-order optical nonlinearity

Figure 4 shows dispersions of the real part, the imaginary part and the absolute value of $\chi^{(3)}(-\omega; 0, 0, \omega)$ for 0.1 to 40 wt% DEANST/PMMA films, which were calculated in the manner described in §2.3. The absolute value of $\chi^{(3)}(-\omega; 0, 0, \omega)$ for the 35 wt% DEANST/PMMA film is 1.6×10^{-12} esu in the nonresonant region (2.1 eV). This value agrees with the value of $\chi^{(3)}(-3\omega; \omega, \omega, \omega) = 2 \times 10^{-12}$ esu at 1.17 eV (1.06 μm) for a 33.5 wt% DEANST/PMMA film

measured by an optical third-harmonic generation technique.[2)]

Using the experimental result of the lowest-concentration sample (0.1 wt%), the averaged third-order hyperpolarizability $\langle\gamma(-\omega; 0, 0, \omega)\rangle$ is evaluated to be 5.8×10^{-35} esu at 2.1 eV. This value is 3.6 times larger than the value of $\langle\gamma(-\omega; 0, 0, \omega)\rangle = 1.602 \times 10^{-35}$ esu at 2.06 eV calculated by an *ab intio* self-consistent-field method.[10)] This deviation is explained as follows. In the far-off-resonant region, where the contribution to the EA signal by the electrostrictive effect becomes significant, the value of $\langle\gamma(-\omega; 0, 0, \omega)\rangle$ from the EA spectroscopy can be overestimated.

Figure 5 shows concentration dependences of the maximum values of $\langle\gamma(-\omega; 0, 0, \omega)\rangle$ and $|\chi^{(3)}(-\omega; 0, 0, \omega)|$. Here we emphasize that $\langle\gamma(-\omega; 0, 0, \omega)\rangle_{\max}$ calculated from the $|\chi^{(3)}(-\omega; 0, 0, \omega)|_{\max}$ decreases with dopant concentration over 10 wt%. Unless the intermolecular interaction is considered, the nonlinearity $\langle\gamma(-\omega; 0, 0, \omega)\rangle$ in a molecule is, in general, independent of the concentration, and hence the macro-nonlinearity $|\chi^{(3)}(-\omega; 0, 0, \omega)|$ is proportional to the concentration.[13)] However, $|\chi^{(3)}(-\omega; 0, 0, \omega)|$ obtained from our experiment is not proportional to the dopant concentration, particularly at high concentrations. Thus, the molecular nonlinearity $\langle\gamma(-\omega; 0, 0, \omega)\rangle$ decreases with concentration. The reason for this behavior will be discussed in §4.

3.3 Evaluation of static dipole-moment difference and static polarizability difference

The absorption spectrum of the charge-transfer molecule is generally so broad that the direct numerical derivative of the absorption spectrum with the measured wavelength resolution of 2 nm becomes very noisy. This makes the analysis using the direct numerical derivatives difficult. In order to avoid this difficulty, we first fit the absorption spectrum to a skewed Gaussian band,[8)]

$$A(E) = b_0 \exp[-(E - E_0)^2/b_1^2 - b_2(E - E_0)^3 - b_3(E - E_0)^4]. \quad (3.2)$$

Secondly, using the derivative from the fitted absorption spectrum, we analyze the EA spectrum. Here, we assume that the component proportional to the absorption spectrum in the measured EA spectrum is negligible, that is, $a_0 = 0$ in eq. (2.7).

For example, Figs. 6(a) and 6(b) show the absorption and EA spectra at the dopant concentration of 0.1 wt%, together with fitting results based on eqs. (2.7) and (3.2). The EA spectrum can be decomposed into the first- and second-derivative components. From these results, the values of $\Delta\mu$ and $\Delta\alpha$ can be evaluated to be 7.7 debye and 2.4×10^{-21} cm^3, respectively. The value of $\Delta\mu$ is somewhat smaller than that for 4-(N,N-dimethylamino)-β-nitrostyrene (DMANST) ($\Delta\mu = 10.3$ debye[4)]) which has almost the similar molecular structure.

Over the dopant concentration of 15 wt%, the measured EA spectra are dissimilar in shape to the first and second

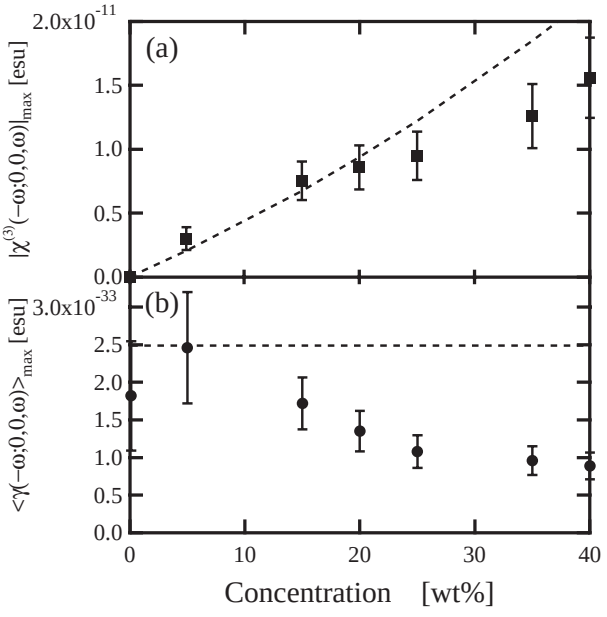

Fig. 5. Concentration dependences of (a) $|\chi^{(3)}(-\omega; 0, 0, \omega)|_{\max}$ and (b) $\langle\gamma(-\omega; 0, 0, \omega)\rangle_{\max}$ for DEANST/PMMA films. Broken lines represent $|\chi^{(3)}(-\omega; 0, 0, \omega)|_{\max}$ and $\langle\gamma(-\omega; 0, 0, \omega)\rangle_{\max}$ value without the intermolecular interaction.

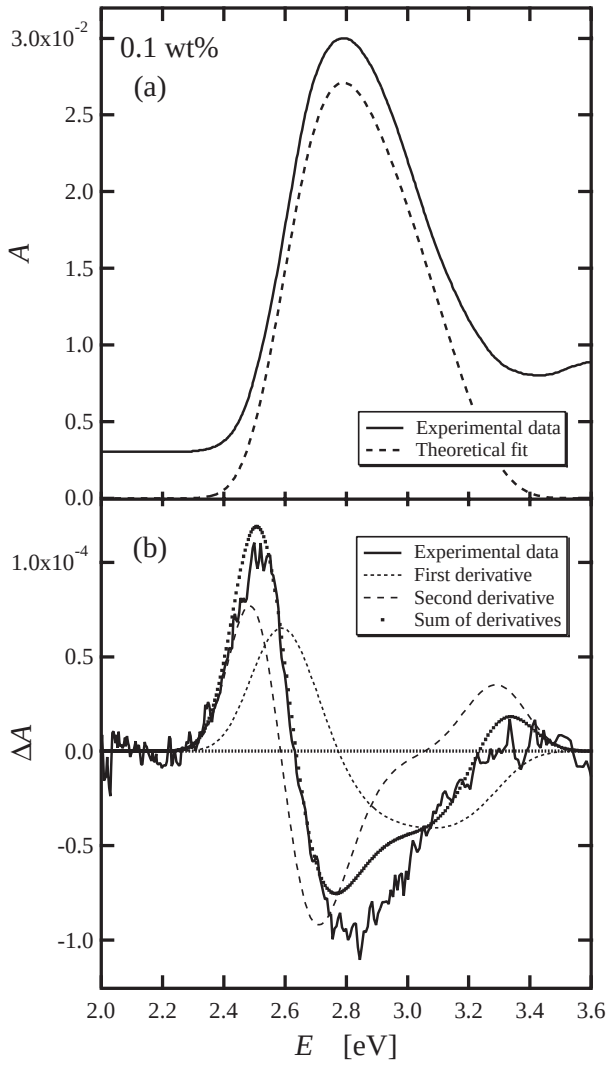

Fig. 6. (a) Absorption spectrum of 0.1 wt% DEANST/PMMA film (solid line) and its theoretical fit (broken line). (b) Electroabsorption spectrum (solid line) and its theoretical fit (dotted line) together with the contribution of the first and second derivatives of the absorption spectrum (broken lines).

derivatives and even their sum. In other words, we cannot fit the EA spectra over the dopant concentration of 15 wt% when we consider only one absorption band. Thus, we decompose the absorption spectra into three bands. For example, Fig. 7 shows the results for the dopant concentration of 35 wt%. Figure 7(a) shows the measured absorption spectrum and the three decomposed absorption bands. The central absorption band has the same shape as the absorption spectrum observed for the lower-concentration samples, namely a skewed Gaussian shape (denoted by A_1). The other absorption bands also have Gaussian shapes (denoted A_2 and A_3 on the lower- and higher-energy sides of the center absorption band, respectively). Figure 7(b) shows the measured and fitted EA spectra with the contributions of first and second derivatives of the three absorption bands. The measured spectrum is reproduced well by the fitting. $\Delta\mu$ and $\Delta\alpha$ values for each absorption band are evaluated using eqs. (2.9) and (2.10).

Figure 8 shows the concentration dependence of the absorption intensities of A_2 and A_3 normalized by that of A_1 (A_2/A_1 and A_3/A_1). Both increase with dopant concentration.

Concentration dependences of $\Delta\mu$ and $\Delta\alpha$ values of the three absorption bands are shown in Fig. 9. It is seen that, with increasing dopant concentration, the values of $\Delta\mu$ decrease while those of $\Delta\alpha$ negligibly change. Moreover, it should be noted that the ratio of the $\Delta\alpha$ value of the A_1 absorption band ($\Delta\alpha_{A_1}$) to that of the A_2 band ($\Delta\alpha_{A_2}$) is about one to two, since this ratio represents the ratio of effective volume size of the species yielding $\Delta\alpha_{A_1}$ to that of the species yielding $\Delta\alpha_{A_2}$.[14)]

3.4 *Picosecond temporal behaviors of emission*

The left-hand side of Fig. 10 shows the emission-decay

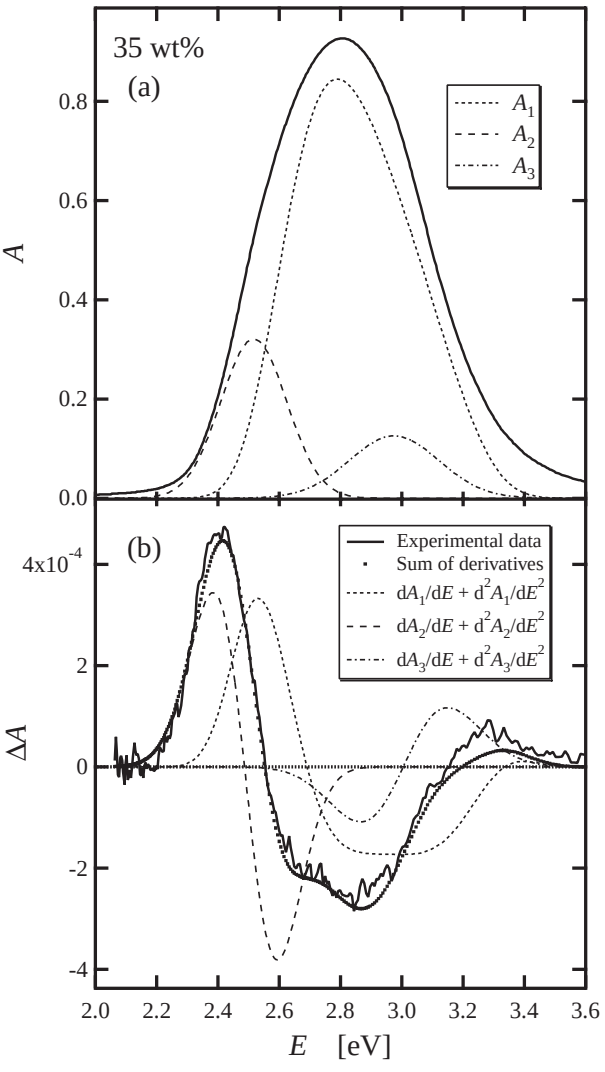

Fig. 7. (a) Absorption spectrum of 35 wt% DEANST/PMMA film (solid line) and three decomposed absorption bands (broken lines). (b) Electroabsorption spectrum (solid line) and its theoretical fit (dotted line) together with the contribution of derivatives of three absorption bands (broken lines).

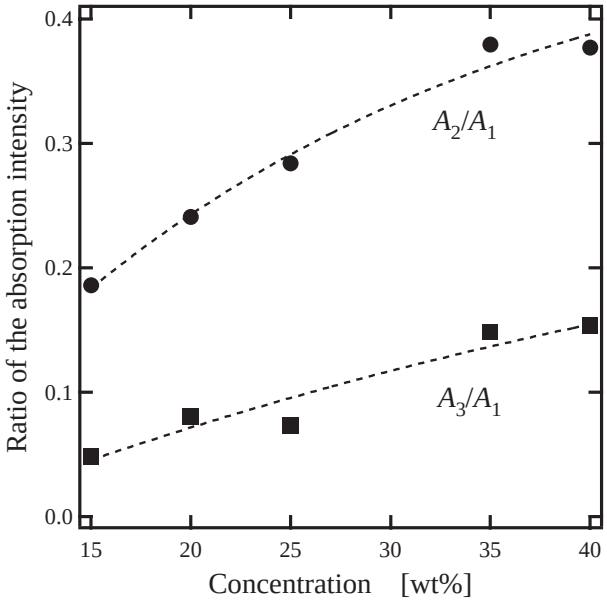

Fig. 8. Dopant concentration dependences of the ratios of the absorption intensities, A_2/A_1 and A_3/A_1.

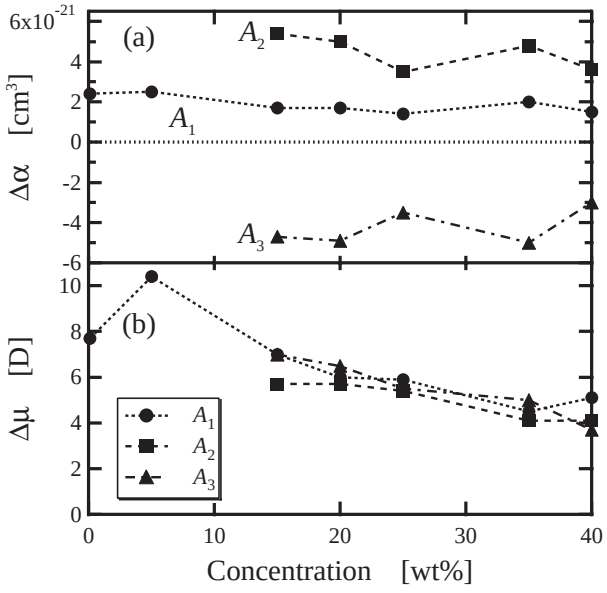

Fig. 9. Dopant concentration dependences of (a) $\Delta\alpha$ and (b) $\Delta\mu$ values of DEANST/PMMA films for the three absorption bands.

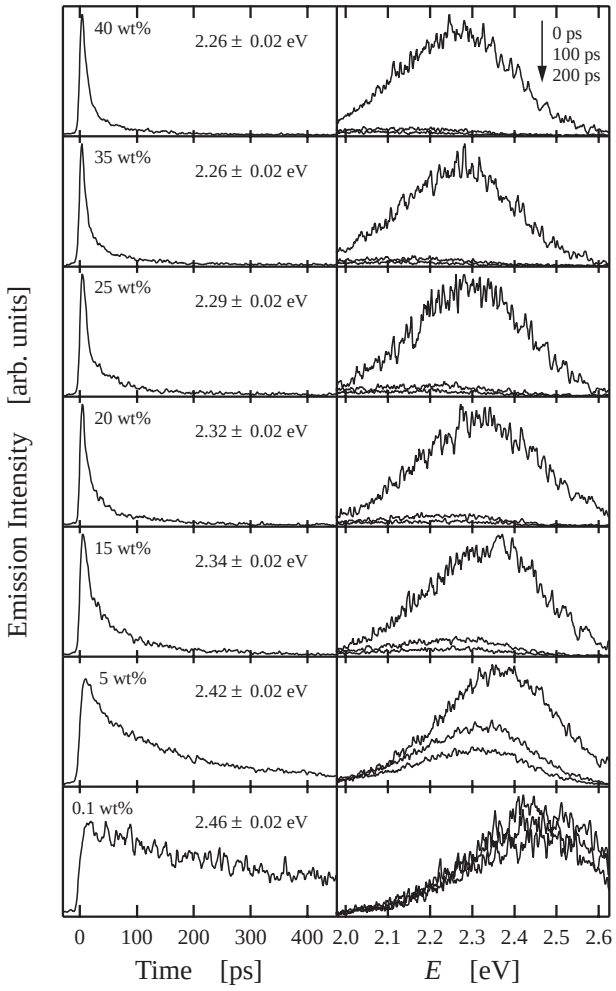

Fig. 10. The emission decay profiles at around the emission peak of E_0 with the energy resolution width $2\Delta E$ of 20 meV in the dopant concentration range of 0.1–40 wt% for DEANST/PMMA films (left-hand side) and corresponding time-resolved emission spectra at $t_0 = 0, 100$ and 200 ps (right-hand side).

profiles $I(t, E_0 \pm \Delta E)$ at around the emission peak of E_0 with the energy resolution width $2\Delta E$ of 20 meV in the dopant concentration range of 0.1–40 wt% for DEANST/PMMA films. The corresponding time-resolved emission spectra $I(t_0 + \Delta t, E)$ at $t_0 = 0, 100$ and 200 ps are also shown on the right-hand side in Fig. 10. The emission decay signals are obtained as an integral with respect to the energy width $2\Delta E$ around E_0 and the time-resolved spectral signals are obtained as an integral during the interval of $\Delta t = 30$ ps from t_0 where the time origin $t_0 = 0$ is set as the arrival time of the excitation pulse peak to the sample.

Emission decay time constants for 0.1 to 40 wt% DEANST-doped PMMA films are listed in Table I. It is found that the emission decay profile in the lowest-concentration sample (0.1 wt%) consists of one component, while the emission in the higher concentration region (not less than 5 wt%) has a fast- and a slow-decay component. The emission-peak photon energy of the fast-decay component is higher than that of the slow-decay component. Both the time constants of the fast- and slow-decay components (τ_1 and τ_2) decrease with dopant concentration. Moreover, the time-resolved emission spectra of both fast- and slow-decay components shift to the lower-energy side with increasing dopant concentration.

Table I. Emission decay constants for 0.1 to 40 wt% DEANST/PMMA films.

Concentration (wt%)	Decay constants (ps) τ_1	τ_2
0.1	510	
5	100	270
15	21	132
20	18	128
25	15	125
35	12	124
40	12	122

4. Discussion

Here, we can summarize the experimental results for DEANST-doped PMMA films as follows: [1] the absorption spectra broaden with increasing dopant concentration, [2] the EA spectra shift to the low-energy side with increasing dopant concentration, [3] the magnitude of the first peak of the EA signals decreases up to 15 wt%, above which it does not change, [4] $\langle\gamma(-\omega; 0, 0, \omega)\rangle_{\max}$ decreases with increasing dopant concentration over 15 wt%, [5] $|\chi^{(3)}(-\omega; , 0, 0, \omega)|_{\max}$ is not proportional to the dopant concentration over 15 wt%, [6] the absorption spectrum consists of three bands over 15 wt% (lower- and higher-energy bands appear), [7] the ratios of both A_2/A_1 and A_3/A_1 increase with dopant concentration, [8] $\Delta\alpha$ negligibly changes with concentration, [9] the ratio between $\Delta\alpha_{A_1}$ and $\Delta\alpha_{A_2}$ is about 1 : 2, [10] $\Delta\mu$ decreases with increasing dopant concentration over 15 wt%, [11] a slow-decay emission band appears on the low-energy side at dopant concentrations greater than 5 wt%, and [12] the emission-decay constant decreases with increasing dopant concentration.

For the two-level model, the average third-order hyperpolarizability $\langle\gamma(-\omega; 0, 0, \omega)\rangle$ and the average linear polarizability $\langle\alpha(-\omega; \omega)\rangle$ are represented by the following equations based on the quantum-mechanical perturbation theory:[15]

$$\langle\gamma(-\omega; 0, 0, \omega)\rangle \propto \frac{1}{\hbar^3}\sum_n |\mu_{ng}|^2(\Delta\mu)^2\left[\frac{1}{(\omega_{ng} - \omega - i\Gamma_{ng})^3} + \frac{1}{(\omega_{ng} + \omega + i\Gamma_{ng})^3}\right], \tag{4.1}$$

$$\langle\alpha(-\omega; \omega)\rangle \propto \frac{1}{\hbar}\sum_n |\mu_{ng}|^2\left(\frac{1}{\omega_{ng} - \omega - i\Gamma_{ng}} + \frac{1}{\omega_{ng} + \omega + i\Gamma_{ng}}\right), \tag{4.2}$$

where μ_{ng} is the electronic transition dipole moment between the excited state n and the ground state g and $\Delta\mu$ is the static-dipole-moment difference denoted in §2.4. Γ_{ng} is the relaxation rate between the excited state and the ground state. $\hbar\omega_{ng}$ is the energy difference between the excited state and the ground state. In the case of the resonant condition, that is, in the case where the excitation photon energy of $\hbar\omega$ is near $\hbar\omega_{ng}$, $\langle\gamma(-\omega; 0, 0, \omega)\rangle$ of eq. (4.1) is reduced to

$$\langle\gamma(-\omega;0,0,\omega)\rangle_{\mathrm{reso}} \propto \frac{1}{\hbar^3}\sum_n \frac{|\mu_{ng}|^2(\Delta\mu)^2}{(\omega_{ng}-\omega-i\Gamma_{ng})^3}. \quad (4.3)$$

In addition, $\langle\alpha(-\omega;\omega)\rangle$ of eq. (4.2) in the low-frequency limit, that is, the average static linear polarizability $\langle\alpha(0;0)\rangle$, is expressed by

$$\langle\alpha(0;0)\rangle \propto \frac{1}{\hbar}\sum_n \frac{2\omega_{ng}|\mu_{ng}|^2}{\omega_{ng}^2+\Gamma_{ng}^2}. \quad (4.4)$$

The molecular hyperpolarizability $\langle\gamma(-\omega;0,0,\omega)\rangle$, which is defined as the nonlinearity in a molecule, is independent of the DEANST concentration, unless the intermolecular interaction is considered. However, the experimental result [4] indicates that DEANST molecules in PMMA film interact with each other and this interaction can influence μ_{ng} and/or $\Delta\mu$. On the other hand, based on the expression of $\langle\alpha(0;0)\rangle$ and the experimental result [8], it is reasonable to say that $|\mu_{ng}|$ or Γ_{ng} negligibly changes with concentration. Thus, it is concluded that the decrease in $\Delta\mu$ with increasing dopant concentration causes the decrease in $\langle\gamma(-\omega;0,0,\omega)\rangle_{\mathrm{max}}$. Furthermore, this explains the experimental result [5] well through eq. (2.5).

Based on the experimental results [3], [4], [6], [7], [10] and [12], we conclude that DEANST molecules aggregate in the PMMA films at concentrations over 5 wt%,[16] and the concentration of aggregates increases with the total DEANST concentration. Thus, this aggregation affects the interaction among DEANST molecules. Consequently, both the absorption spectrum and the EA spectrum change and $\Delta\mu$ or $\langle\gamma(-\omega;0,0,\omega)\rangle$ decreases with increasing dopant concentration. This is supported by the experimental results [1], [2] and [11]. Moreover, the experimental result [9] suggests that the aggregate is a dimer.

On the basis of these results and Kasha's theory of aggregates,[17] the origin of new absorption bands and the mechanism of the excited-state energy relaxation with two emission bands at high dopant concentrations are understood as follows. Figure 11 shows the probable energy diagram of DEANST/PMMA films in the high concentration region. In this concentration region, both monomers and dimers of DEANST molecules coexist. The monomer level is split into two levels by the formation of aggregates. The lower energy level (A_2) is mainly dipole-transition-allowed, but the higher energy level (A_3) is partially dipole-transition-allowed. The emission of DEANST/PMMA films with the lowest concentration is from the monomer level (A_1) and the relaxation rate (τ_1^{-1}) is slow. DEANST molecules begin to aggregate at about 5 wt% concentration and the concentration of dimers increases with the total DEANST concentration. Thus, the relaxation rate of monomers rapidly becomes faster with increasing dopant concentration because of the energy transfer from monomers to dimers. Since the energy position of the emission from dimers is on the lower-energy side of that from monomers, the relaxation from the lower level of dimer is slower than that from the monomer level. The relaxation rate of dimers (τ_2^{-1}) also becomes faster with increasing dopant concentration due to the energy transfer between dimers.

It follows from the discussion above that the $\langle\gamma(-\omega;0,0,\omega)\rangle$ values in the higher concentration region evaluated in this study are the effective values of $\langle\gamma(-\omega;0,0,\omega)\rangle$ ($\langle\gamma(-\omega;0,0,\omega)\rangle_{\mathrm{eff}}$). That is,

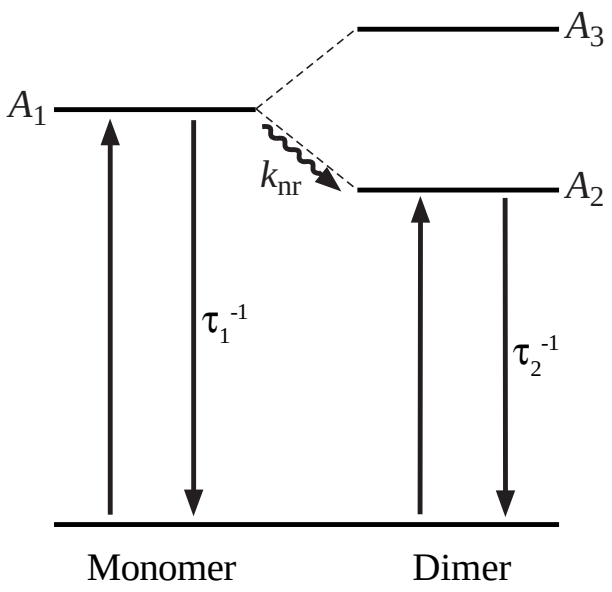

Fig. 11. The energy diagram of DEANST/PMMA film in the higher concentration region. k_{nr} is the nonradiative relaxation rate from A_1 to A_2. τ_1^{-1} and τ_2^{-1} are the emittive relaxation rates from A_1 to ground state and A_2 to ground state, respectively.

$\langle\gamma(-\omega;0,0,\omega)\rangle_{\mathrm{eff}}$ is defined to be the third-order nonlinearity per monomer molecule whether DEANST molecules aggregate or not.

5. Conclusion

We measured the absorption and EA spectra for DEANST-doped PMMA films in the dopant concentration range of 0.1–40 wt%. From these results, we calculated the dispersion of the third-order nonlinear optical susceptibility $\chi^{(3)}(-\omega;0,0,\omega)$ using the Kramers-Kronig relation. In addition, we evaluated the static polarizability difference $\Delta\alpha$ and the static dipole-moment difference $\Delta\mu$. Furthermore, we measured the picosecond emission-decay profiles and the time-resolved emission spectra for DEANST-doped PMMA films at 0.1–40 wt% concentrations. Consequently it was found that the absorption spectrum, the EA spectrum, the time-resolved emission spectrum, the maximum third-order susceptibility, the maximum hyperpolarizability and the permanent dipole-moment difference, except for the linear polarizability difference, significantly change at dopant concentrations over 5 wt%.

From these experimental results, we concluded that DEANST molecules in PMMA films aggregate at concentrations over 5 wt%. This aggregation gives rise to two new absorption bands. In addition, the intermolecular interaction affected by the aggregation causes a decrease in $\Delta\mu$ and $\langle\gamma(-\omega;0,0,\omega)\rangle_{\mathrm{eff}}$, and the nonproportional behavior of $|\chi^{(3)}(-\omega;0,0,\omega)|$ with increasing dopant concentration. Furthermore, this aggregation explains the absorption spectral change, the EA spectral shift and the appearance of two emission-decay constants with increasing dopant concentration. Finally, we evaluated the average aggregation number of DEANST molecules to be two which suggests that DEANST molecules in PMMA films form dimers at concentrations over 5 wt%.

1) T. Kurihara, H. Kanbara, H. Kobayashi, K. Kubodera, S. Matsumoto and T. Kaino: Opt. Commun. **84** (1991) 149.
2) T. Kaino, T. Kurihara, K. Kubodera and H. Kanbara: *Materials for Nonlinear Optics*, eds. S. Marder, J. E. Sohn and G. D. Stucky (American Chemical Society, Washington, DC, 1991) p. 704.
3) R. Gadonas: *J-aggregates*, ed. T. Kobayashi (World Scientific, Singapore, 1996) p. 181.
4) W. Liptay: *Excited States*, ed. E. C. Lim (Academic Press, New York, 1974) p. 129.
5) T. Wada, T. Masuda and H. Sasabe: Mol. Cryst. & Liq. Cryst. **247** (1994) 139.
6) W. Jia, K. Misawa, H. Matsuda, S. Okada, H. Nakanishi and T. Kobayashi: Chem. Phys. Lett. **255** (1996) 385.
7) T. Fujiwara, Y. Kamoshida, R. Morita and M. Yamashita: J. Photochem. Photobiol. B **41** (1997) 114.
8) D. H. Oh, M. Sano and S. G. Boxer: J. Am. Chem. Soc. **113** (1991) 6880.
9) J. R. Reimers and N. S. Hush: J. Phys. Chem. **95** (1991) 9773.
10) V. Keshari, S. P. Karna and P. N. Prasad: J. Phys. Chem. **97** (1993) 3525.
11) S. J. Lalama and A. F. Garito: Phys. Rev. A **20** (1979) 1179.
12) V. L. Colvin, K. L. Cunningham and A. P. Alivisatos: J. Chem. Phys. **101** (1994) 7122.
13) In a strict sense, since refractive index $n(\omega)$ or Lorentz local field factor $L(\omega)$ depends on the dopant concentration, $|\chi^{(3)}(-\omega; 0, 0, \omega)|_{\max}$ is not proportional to the dopant concentration. Thus, the broken line for $|\chi^{(3)}(-\omega; 0, 0, \omega)|_{\max}$ values without the intermolecular interaction is slightly curved, not linear. However, even in the case of considering the concentration dependence of $L(\omega)$ in the DEANST/PMMA films, $|\chi^{(3)}(-\omega; 0, 0, \omega)|_{\max}$ can be regarded as almost proportional to the dopant concentration.
14) K. Misawa and T. Kobayashi: Nonlinear Opt. **14** (1995) 103.
15) R. W. Boyd: *Nonlinear Optics* (Academic Press, Boston, 1992) p. 101.
16) The evaluation of the concentration beginning with the aggregation (C_a) by means of the absorption and EA measurements differs from that of the emission measurements. This is due to the fact that the latter measurements are more sensitive than the former ones. Therefore, we evaluated C_a to be 5 wt% by the latter measurement.
17) M. Kasha: Radiat. Res. **20** (1963) 55.